JURNAL INFOTEL
VOL. 18, NO. 4, NOVEMBER 2026, PP. 555–576. DOI:10.20895/INFOTEL.V18I4.11638

RESEARCH ARTICLE

SDR-Based Infrared Optical Wireless Communication System for LiFi Uplink

Eril Mozef[1,*], Naufal Daffa Naafilah[2], Hepi Ludiyati[3], and Enceng Sulaeman[4]

[1,2,3,4]Department of Electrical Engineering, Politeknik Negeri Bandung, 40559, Indonesia

*Corresponding email: emozef@polban.ac.id

Received: July 01, 2026; Revised: September 01, 2026; Accepted: September 11, 2026.

Abstract: Optical Wireless Communication (OWC) using the infrared (IR) spectrum has emerged as a promising alternative for uplink LiFi systems due to its immunity to electromagnetic interference and reduced radio-frequency spectrum congestion. Existing SDR-based LiFi/OWC implementations have primarily focused on communication performance using specific optical configurations or test signals, with limited emphasis on end-to-end multimedia transmission under varying illumination conditions. This study presents the design, implementation, and experimental evaluation of an SDR-based infrared LiFi uplink system that integrates GNU Radio, HackRF One, an $850\,\mathrm{nm}$ VCSEL, and a BPW34 photodiode for end-to-end transmission of text, audio, and image data. BPSK modulation is employed, and the system is evaluated under indoor illumination levels up to $800\,\mathrm{lux}$ and outdoor solar illumination levels up to $50{,}000\,\mathrm{lux}$, with transmission distances from 10 to $70\,\mathrm{cm}$. Reliable multimedia transmission is achieved within the operating range 10– $60\,\mathrm{cm}$, with an average BER of 9.41×10^{-5} and a maximum effective throughput of $94.60\,\mathrm{kbps}$. At $70\,\mathrm{cm}$, reduced received optical power and increased ambient optical noise degrade communication performance and multimedia data integrity. The results demonstrate the practical feasibility of a low-cost SDR-based infrared LiFi uplink platform for short-range multimedia communication under varying ambient lighting conditions.

Keywords: LiFi, infrared uplink, GNU radio, VCSEL, BPSK, optical wireless communication

1 Introduction

Optical Wireless Communication (OWC) has emerged as a promising wireless communication technology that utilizes the optical spectrum as a transmission medium for high-capacity and high-speed data transmission systems [1], [2], [3], [4]. Among various OWC

© Jurnal Infotel ISSN: 2085-3688; e-ISSN: 2460-0997

implementations, Light Fidelity (LiFi) has gained significant attention due to its ability to provide bidirectional wireless communication with high spectral efficiency, low latency, and improved physical-layer security compared to conventional radio-frequency-based communication systems [5], [6]. In practical LiFi architectures, visible light is commonly utilized for downlink transmission, while infrared (IR) communication is considered more suitable for uplink implementation because it eliminates visual disturbances for users and enables more flexible optical channel deployment [7], [8].

Despite its advantages, LiFi uplink systems based on infrared still face several technical challenges associated with optical channel stability and environmental interference. Ambient illumination and solar radiation can introduce significant optical noise into the receiver, resulting in Signal-to-Noise Ratio (SNR) degradation and increased Bit Error Rate (BER) performance [4], [9], [10]. In addition, the performance of digital optical communication systems strongly depends on the stability of phase synchronization during carrier recovery and demodulation processes. Optical signal attenuation caused by propagation distance, random orientation, and environmental interference may lead to phase lock degradation in Costas Loop-based synchronization systems [11], [12], ultimately affecting communication reliability and real-time data reconstruction. Therefore, selecting a modulation scheme with strong robustness against optical noise and synchronization disturbances is essential for reliable infrared uplink communication.

Several digital modulation techniques have been investigated for Optical Wireless Communication systems to improve transmission reliability under noisy optical environments [13], [14]. Among these techniques, Binary Phase Shift Keying (BPSK) offers good BER performance under low SNR conditions while maintaining relatively simple implementation complexity compared to higher-order modulation schemes [11], [13]. The robustness of BPSK against phase-related impairments makes it suitable for infrared-based optical wireless communication systems operating under varying ambient light conditions and synchronization instability.

Previous studies have demonstrated significant advances in Optical Wireless Communication (OWC) and Light Fidelity (LiFi) technologies. Yu et al. [1] reviewed the development of Visible Light Communication (VLC) systems by discussing optical devices, system architectures, and practical applications for future wireless communications. Complementing this work, Chowdhury et al. [4] presented a comprehensive survey of optical wireless hybrid networks, highlighting their opportunities, technical challenges, and future research directions. Focusing on infrared communication, Chen et al. [7] investigated infrared-based LiFi uplink transmission under link blockage and random device orientation, demonstrating the feasibility of infrared communication for reliable uplink applications. Liu et al. [11] further implemented a real-time hybrid visible light/infrared communication system capable of supporting full-range dynamic dimming control, demonstrating the practicality of integrating visible and infrared optical links in real-time applications. In addition, Cheng et al. [15] reviewed recent advances in $850\,\mathrm{nm}$ Vertical-Cavity Surface-Emitting Lasers (VCSELs) for high-speed optical interconnects, while Mozef et al. [16] demonstrated the hardware implementation of RF-to-Optical and Optical-to-RF converters for a laser-driven VLC system based on HackRF One SDR, confirming the feasibility of software-defined optical wireless communication.

Although these studies have demonstrated the feasibility of infrared communication, VCSEL-based optical transmitters, and SDR-enabled optical wireless systems, several limitations remain. Most existing implementations are still confined to simulations, controlled

laboratory environments, or dedicated hardware platforms with limited flexibility [11,16]. Moreover, the real-time implementation of LiFi uplink systems based on infrared using low-cost Software Defined Radio (SDR) platforms remains relatively underexplored, particularly for multimedia communication applications under high-intensity ambient light conditions [16]. Comprehensive investigations involving synchronization stability, Bit Error Rate (BER), throughput performance, and real-time multimedia reconstruction under outdoor solar interference are also rarely reported in the existing literature [7], [11], [16]. To address these gaps, this study develops and experimentally evaluates a low-cost software-defined infrared LiFi uplink system based on GNU Radio, HackRF SDRs, a $850\,\mathrm{nm}$ VCSEL and a BPW34 photodiode. Rather than claiming novelty from the individual use of SDR, GNU Radio, BPSK, or optical components, the contribution of this work lies in their integration into an end-to-end infrared LiFi uplink platform and its comprehensive experimental characterization under varying transmission distances and ambient illumination conditions. The main contributions of this study are as follows.

1. A low-cost SDR-based infrared LiFi uplink transceiver is implemented using GNU Radio, HackRF One, HackRF PortaPack H4M and an optical front-end $850\,\mathrm{nm}$ VCSEL-BPW34 for end-to-end digital multimedia transmission.
2. A complete experimental characterization of the proposed system is conducted in indoor and outdoor environments by evaluating the SNR, BER, effective throughput, synchronization behavior, constellation characteristics, and multimedia data reconstruction over transmission distances of 10–$70\,\mathrm{cm}$ under different ambient illumination conditions.
3. The practical operating boundary of the proposed LiFi infrared uplink is experimentally identified by analyzing the relationship between transmission distance, ambient illumination, communication quality, and multimedia data integrity. The results establish a reliable operating range of 10–$60\,\mathrm{cm}$ and characterize the performance degradation observed at $70\,\mathrm{cm}$.

2 Research Method

This section describes the architectural design, realization, and experimental testing of the proposed OWC transceiver system. The system integration and technical overview are detailed in the following subsections.

2.1 System Design and Implementation

2.1.1 SDR-Based Uplink LiFi System Architecture

The complete signal path of the proposed infrared LiFi uplink system consists of digital baseband processing, RF-to-optical conversion, free-space optical transmission, optical-to-electrical conversion, and digital baseband recovery. At the transmitter, the multimedia data are processed in GNU Radio, where the input data are packetized and modulated using BPSK. The resulting digital baseband signal is converted into an RF signal by the HackRF One SDR. The generated $10\,\mathrm{MHz}$ RF signal is then delivered to the optical transmitter front-end, where the RF signal is coupled to the bias circuit and drives the $850\,\mathrm{nm}$

VCSEL. The VCSEL converts the electrical modulation signal into an intensity-modulated infrared optical signal that propagates through the free-space optical channel.

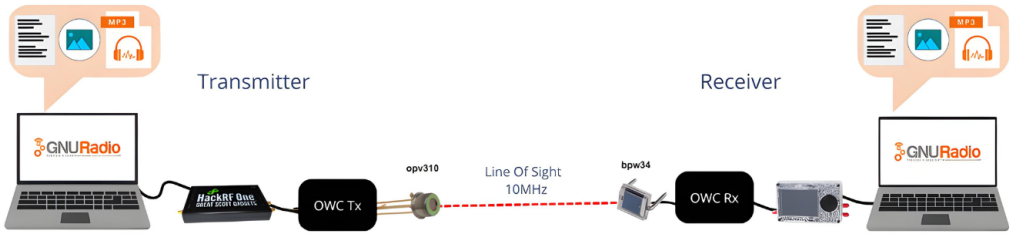

Figure 1: Proposed SDR-based uplink LiFi transceiver architecture.

At the receiver, the transmitted infrared optical signal is detected by the BPW34 photodiode, which converts the incident optical power into a photocurrent. The optical front-end of the receiver converts this photocurrent into an electrical signal while separating the information-bearing AC component from the DC component associated with the optical bias and ambient illumination. The recovered electrical signal is subsequently supplied to the HackRF PortaPack H4M SDR for digitization and transfer to the host computer. In GNU Radio, the received signal undergoes the corresponding filtering, symbol synchronization, carrier phase recovery using the Costas Loop, BPSK demodulation, and packet decoding processes. The CRC32 mechanism is then used to validate the received packets before the recovered payload is reconstructed into the original digital multimedia files.

2.1.2 Optoelectronic Component Selection

The selection of optoelectronic components is based on the spectral compatibility between the optical transmitter and receiver to minimize the loss of spectral mismatch. Figure 2 presents the wavelength-dependent characteristics of the selected devices. As shown in Figure 2(a), the OPV310 VCSEL was chosen as the optical transmitter due to its emission wavelength of $850\,\mathrm{nm}$ and rise time/fall time of approximately $100\,\mathrm{ps}$, which makes it suitable for high-speed intensity modulation.

On the receiver side, the BPW34 photodiode was selected because its peak responsivity lies within the $850 - \text{-}950\,\mathrm{nm}$ spectral range, providing good spectral overlap with the emission wavelength OPV310, as shown in Figure 2(b). Although its response time is shorter than that of dedicated high-speed photodetectors, the BPW34 offers relatively high responsivity and a large active area, which facilitate optical alignment and provide sufficient received signal levels for the initial characterization of the uplink LiFi system.

2.1.3 Optical Front-End Circuit Design and SDR Interfacing

This subsection presents the design of the Bias-Tee network used to interface the software-defined radio (SDR) platform with the optoelectronic front-end operating at a $10\,\mathrm{MHz}$ subcarrier frequency. The complete transmitter (Tx) and receiver (Rx) circuits are illustrated in Figure 3.

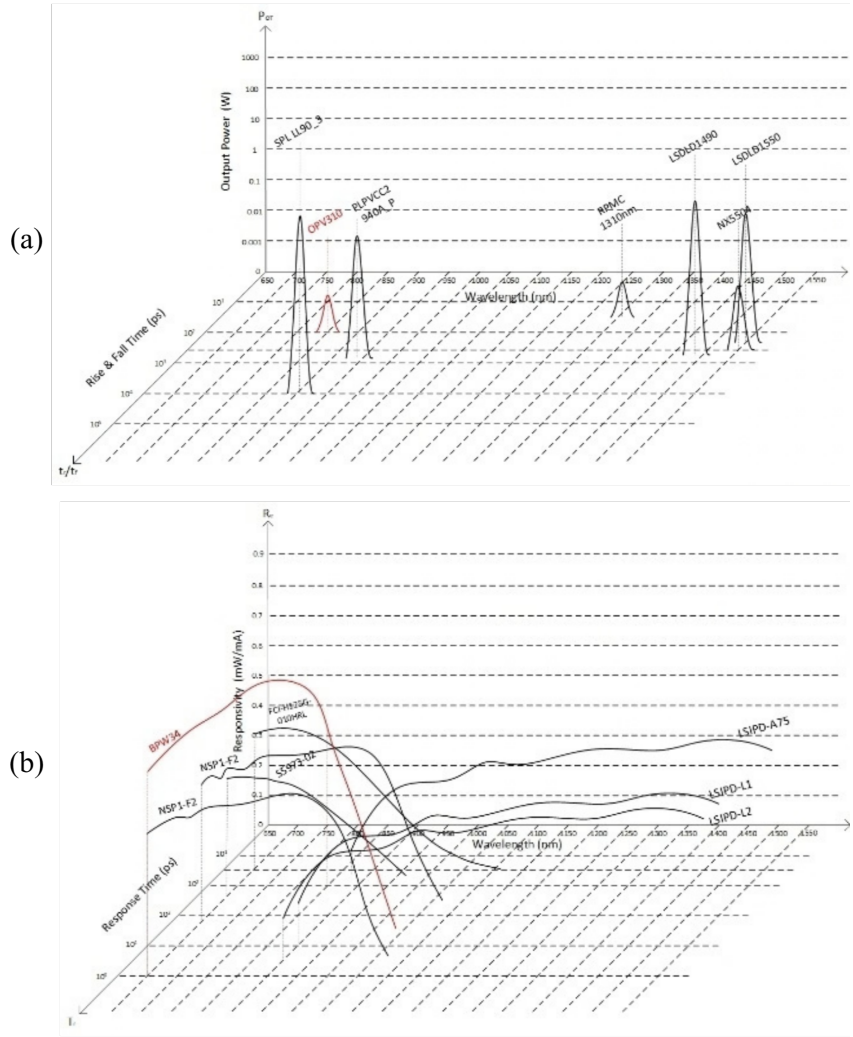

Figure 2: Optoelectronic spectral characteristics: (a) optical emission spectrum of the OPV310 VCSEL and (b) spectral responsivity of the BPW34 photodiode.

At the transmitter side, the $10\,\mathrm{MHz}$ RF signal generated by the HackRF One is coupled through the capacitor (C_{Tx}), which acts as a DC-blocking element while allowing the RF signal to pass with minimal attenuation. To ensure efficient RF coupling, the capacitor is selected to exhibit low capacitive reactance at the operating frequency, as described by Eq.(1):

$$X_C = \frac{1}{2\pi f C} \tag{1}$$

where (X_c) is the capacitive reactance, (f) is the operating frequency, and (C) is the capacitance.

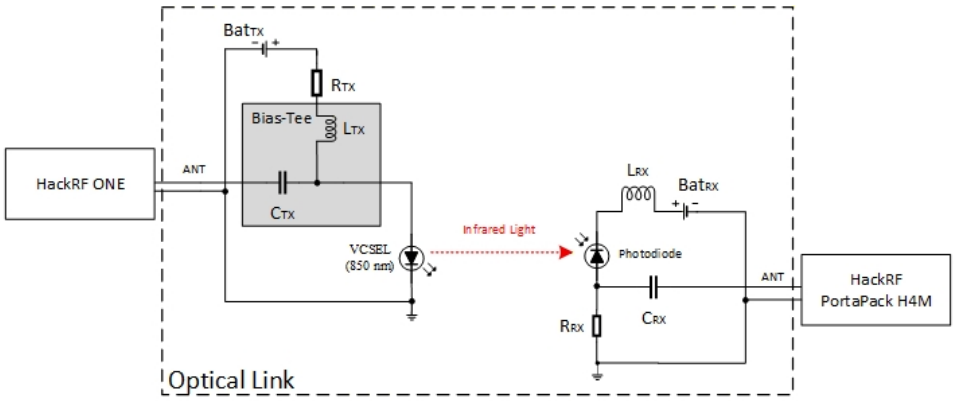

Figure 3: Schematic of the proposed SDR-based uplink LiFi transceiver front-end.

A Bias-Tee network formed by (C_{Tx}) and (L_{Tx}) combines the RF modulation signal with the DC bias current required by the $850\,\mathrm{nm}$ OPV310 VCSEL. The inductor is designed to provide high inductive reactance at the operating frequency, as expressed by Eq.(2):

$$X_L = 2\pi f L \tag{2}$$

where (X_L) is the inductive reactance, (f) is the operating frequency, and (L) is the inductance.

In addition, the resistor (R_{Tx}) serves as a current-limiting resistor to regulate the VCSEL bias current according to Ohm's law, as described by Eq.(3):

$$I_F = \frac{V_{\mathrm{BatTx}} - V_F}{R_{\mathrm{Tx}}} \tag{3}$$

where (I_F) is the forward current of VCSEL, (V_{BatTx}) is the DC voltage supplied by the transmitter battery, (V_F) is the forward voltage of VCSEL and R_{Tx} is the current limiting resistance. The RF modulation signal and the DC bias current are then combined by the Bias-Tee network to drive the intensity modulation of the VCSEL before the optical signal is transmitted through the optical channel.

On the receiver side, the BPW34 photodiode converts the received optical signal into a photocurrent, which is transformed into a voltage signal through the load resistor (R_{Rx}). The resistor R_{Rx} therefore functions as the photodiode load to convert the generated photocurrent into a measurable voltage signal. The capacitor (C_{Rx}) couples the information-bearing AC component while suppressing the DC component introduced by biasing and ambient illumination. Similarly to the transmitter, the capacitor is selected to provide a low capacitive reactance at the operating frequency according to Eq.(1). Meanwhile, the inductor (L_{Rx}) provides isolation between the RF signal path and the bias supply by presenting high inductive reactance, as described by Eq.(2). The recovered electrical signal is subsequently delivered to the receiving SDR for digitization and further baseband processing.

The transmitter and receiver optical front-ends are directly interfaced with the SDR platforms to form the complete electrical-to-optical and optical-to-electrical signal paths. At the transmitter, the modulated RF signal generated by the HackRF One is coupled to the

VCSEL through the bias-tee network, where the electrical RF signal is superimposed on the DC bias and converted into an intensity modulated infrared optical signal. At the receiver, the BPW34 converts the incident optical signal into a photocurrent, which is subsequently converted into an electrical signal and coupled to the RF input of the HackRF PortaPack H4M. The digitized signal is then transferred to the host computer for baseband processing in GNU Radio.

The SDR platforms provide the interface between the software-based digital signal processing and the optoelectronic front-end. The GNU Radio flowgraph generates the BPSK modulated signal at the transmitter and processes the received signal at the receiver, while the HackRF devices perform the corresponding RF signal generation and digitization. This configuration allows the digital processing functions to be implemented through software, while the optical signal conversion and biasing functions are performed by the dedicated VCSEL and photodiode-based hardware. The detailed implementation of the BPSK modulation, synchronization, carrier recovery, and data recovery processes is presented in subsubsection 2.1.4.

2.1.4 GNU Radio BPSK Flowgraph

The GNU Radio framework is employed to implement packet generation, synchronization, modulation, and signal recovery functions for the proposed SDR-based LiFi transceiver. Based on the architecture based on the reference packet [17], the original flowgraph was adapted to interface directly with the optoelectronic front-end.

BPSK modulation is employed in the proposed system as a binary modulation scheme with one bit per symbol. The modulation is implemented in the electrical/RF signal-processing chain using GNU Radio and the HackRF One, while the optical link operates on the basis of intensity modulation and direct detection (IM/DD). The BPSK-modulated electrical signal is applied to $850\,\mathrm{nm}$ VCSEL through the optical transmitter front-end, producing the corresponding variations in the emitted optical intensity. The modulated optical signal is detected by the BPW34 photodiode and converted back into an electrical signal for subsequent BPSK recovery at the receiver. Thus, BPSK processing is performed in the electrical/RF domain, while the VCSEL–photodiode link operates through optical intensity modulation and direct detection. The corresponding transmitter and receiver implementations in GNU Radio are illustrated in Figure 4 and Figure 5, respectively.

At the transmitter side (Figure 4), the multimedia data is segmented into fixed-length payloads and encapsulated into transmission frames with a total frame length of $338\,\mathrm{bytes}$. The generated frames are subsequently mapped into BPSK symbols using the GNU Radio Constellation Modulator block and transmitted through the SDR platform. Differential encoding is enabled within the Constellation Modulator to mitigate phase ambiguity during carrier recovery and improve synchronization robustness. The packet-based BPSK architecture was adapted from the GNU Radio file-transfer framework [17], while the digital processing chain was interfaced with the proposed optical front-end.

A $10\,\mathrm{MHz}$ subcarrier frequency is used for transmission, corresponding to the designed operating frequency of the RF-to-optical front-end. The Bias-Tee and optoelectronic interfaces are designed to operate at this frequency, allowing the RF modulation signal generated by the SDR to be coupled to the VCSEL.

A sampling rate (f_s) of $2\,\mathrm{MSps}$ is used with a Samples-per-Symbol (SPS) value of 4. Since BPSK conveys one bit per symbol and the target gross bit rate is $500\,\mathrm{kbps}$, the corre-

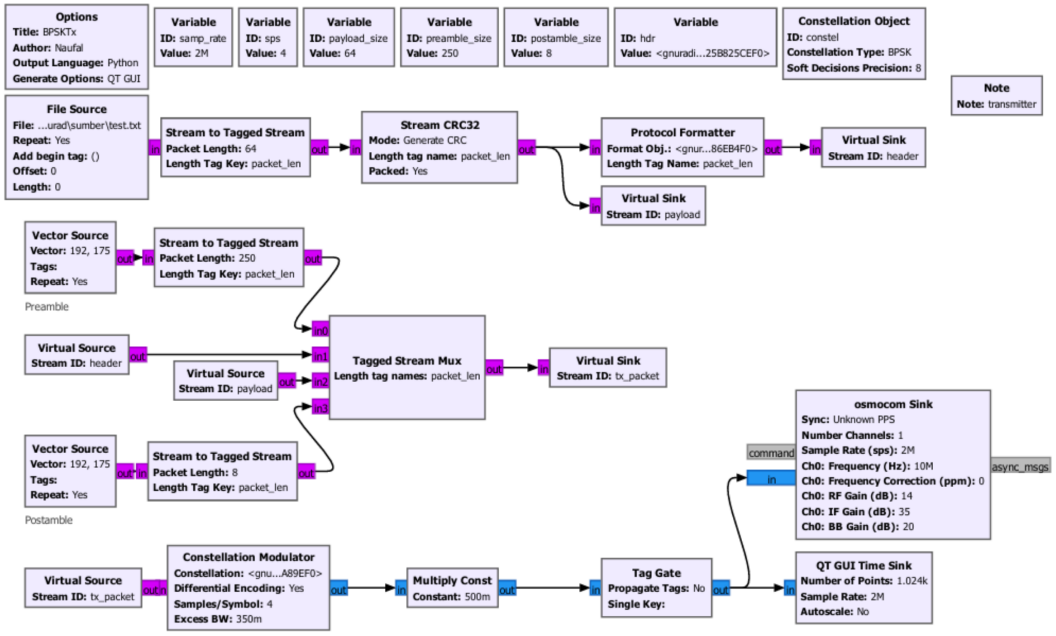

Figure 4: GNU Radio transmitter flowgraph of the proposed BPSK-based uplink LiFi system.

sponding symbol rate (R_s) is $500\,\mathrm{ksymbol/s}$. With four samples per symbol, the required sampling rate is therefore $2\,\mathrm{MSps}$, as expressed by Eq.(4):

$$R_s = \frac{f_s}{SPS} \tag{4}$$

where (R_s) is the symbol rate, (f_s) is the sampling rate and (SPS) is the number of samples per symbol. Thus,

$$R_s = \frac{2\,\mathrm{MSps}}{4} = 500\,\mathrm{ksymbol/s} \tag{5}$$

Since BPSK conveys one bit per symbol, the corresponding gross bit rate is $500\,\mathrm{kbps}$. This gross rate represents the physical-layer transmission rate before accounting for packet framing and other protocol-related overhead. The same digital signal-processing configuration was maintained throughout the experiments to ensure consistent evaluation across different transmission distances and illumination conditions.

On the receiver side (Figure 5), the received signal is first passed through a Root Raised Cosine (RRC) filter to suppress out-of-band noise and perform pulse shaping. A Symbol Synchronizer block is then applied to recover the symbol timing, followed by a Costas Loop for carrier phase recovery. The synchronized signal is subsequently processed by the Constellation Decoder and Differential Decoder blocks to recover the transmitted binary data. The recovered bitstream is passed through a Stream to Tagged Stream block and a Stream CRC32 block to validate packet integrity. Finally, the Repack Bits block reconstructs the original byte stream which is written to the corresponding file format using the File Sink block.

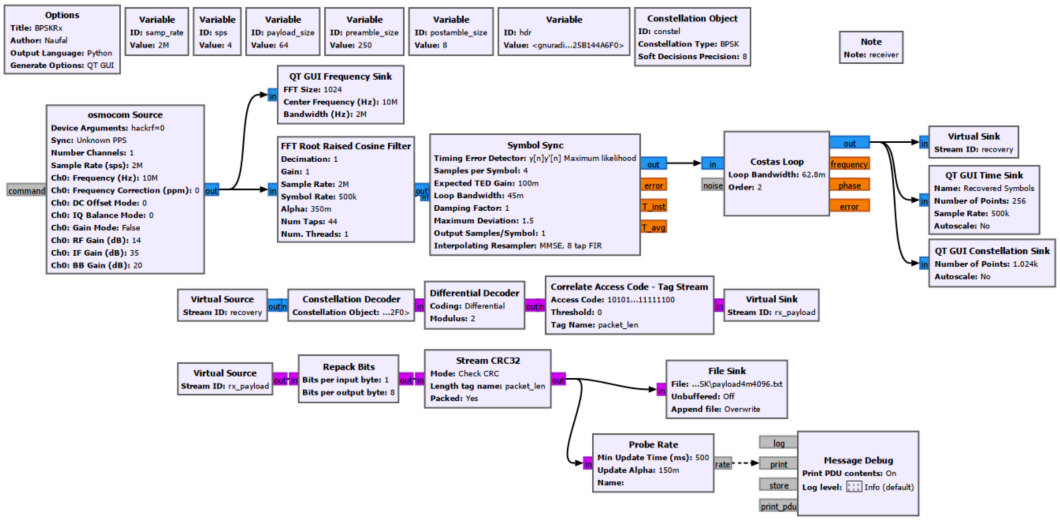

Figure 5: GNU Radio receiver flowgraph of the proposed BPSK-based uplink LiFi system.

2.2 Experimental Setup

2.2.1 Hardware Integration and Alignment

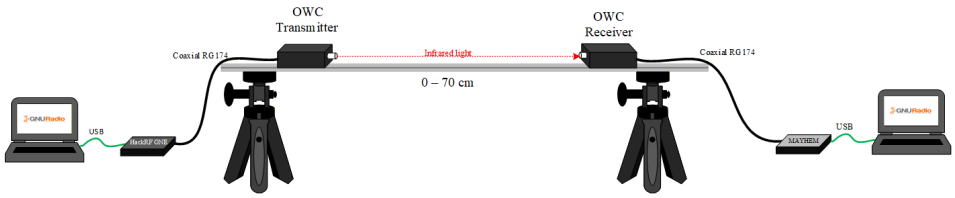

Figure 6: Experimental setup of the proposed SDR-based infrared OWC transceiver.

Experimental evaluation of the proposed OWC system is conducted using an end-to-end experimental setup mounted on a mechanical rail to maintain line-of-sight (LoS) alignment between the transmitter and receiver modules and to allow systematic adjustment of the transmission distance. The experimental configuration is illustrated in Figure 6, while photographs of the implemented configuration are shown in Figure 7. At the transmitter side, a host computer running GNU Radio interfaces with a HackRF One SDR, which generates the modulated 10 MHz RF signal and forwards it to the optical transmitter through an RG-174 coaxial cable. The modulated optical signal propagates through free space toward the receiver side. At the receiver side, the recovered electrical signal is delivered to a HackRF PortaPack H4M SDR and subsequently transferred to the host computer for real-time demodulation and performance analysis.

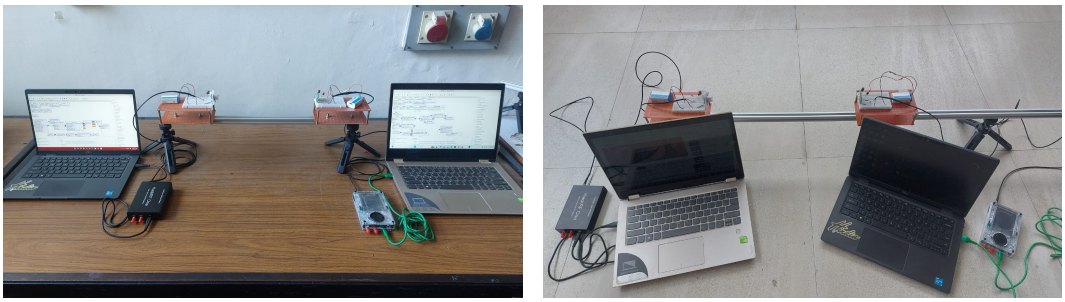

(a) (b)

Figure 7: Photographs of the experimental setup under (a) indoor and (b) outdoor testing environments.

2.2.2 Indoor Experimental Scenario

Indoor experiments were conducted under three nominal ambient illumination conditions of 0, 300, and 800 lux. The 0-lux condition represented a completely dark environment, while the 300-lux condition represented room lighting. The 800-lux condition represented room lighting combined with additional daylight entering through a window during daytime. Because ambient illumination could fluctuate during the measurements, the reported illumination levels represent the nominal conditions used to categorize the experimental measurements. These conditions were used to characterize system performance under progressively increasing indoor ambient illumination. To evaluate transmission performance under varying channel conditions, the multimedia files listed in Table 1 were transmitted sequentially using the GNU Radio architecture.

Table 1: Specifications of the multimedia test files

No.	Data Type	File Format	File Size
1	Text	*.txt	995 KB (1,019,840 B)
2	Audio	*.mp3	4.39 MB (4,610,644 B)
3	Image	*.png	827 KB (847,486 B)

Performance metrics, including Signal-to-Noise Ratio (SNR), Bit Error Rate (BER), effective throughput, and recovered data integrity, were recorded at each measurement point. The receiver position was incrementally adjusted from 10 cm to 70 cm in 10 cm steps to characterize the distance-dependent communication performance and identify the practical operating limit of the system while maintaining LoS alignment.

2.2.3 Outdoor Experimental Scenario

Outdoor experiments were conducted directly under sunlight and evaluated under three nominal solar illumination conditions of 10,000, 25,000, and 50,000 lux. Because solar illumination can vary during the measurements due to changes in sunlight conditions, the reported illumination levels represent the nominal conditions used to categorize the experimental measurements. The 10,000-lux condition represented a relatively low-intensity sun-

light condition, the 25,000-lux condition represented a moderate sunlight condition, and the 50,000-lux condition represented a high-intensity sunlight condition measured around noon. These conditions were selected to characterize the effect of increasing direct solar illumination on the optical communication link. The same multimedia data set, SDR parameters, modulation configuration, and measurement procedures used in the indoor experiments were maintained to ensure a consistent comparison. The distance of separation between transmitter and receiver was varied from 10 cm to 70 cm using the mechanical rail system, and the performance of the system was evaluated in terms of SNR, BER, effective throughput, and data reconstruction.

3 Results

This section presents the experimental results obtained from the proposed SDR-based Optical Wireless Communication (OWC) uplink system employing Binary Phase Shift Keying (BPSK) modulation. The experimental evaluation consists of multimedia transmission validation and communication performance analysis under both indoor and outdoor environments. The system was evaluated over transmission distances ranging from 10 cm to 70 cm under different levels of ambient illumination. The multimedia transmission results are first presented to verify the end-to-end functionality of the proposed system, followed by a detailed communication performance analysis based on Signal-to-Noise Ratio (SNR), Bit Error Rate (BER), throughput, and constellation characteristics.

Table 2 presents the end-to-end validation results for multimedia transmission at the recommended operating distance of 60 cm. The transmitted and received multimedia files are compared in terms of file size, successful reconstruction, and observable data integrity. The results confirm that all multimedia payloads were successfully reconstructed at the receiver without observable corruption or data modification, demonstrating that the proposed SDR-based OWC system is capable of reliably supporting real-time multimedia transmission under the recommended operating conditions.

Table 3 summarizes the average communication performance of the proposed SDR-based OWC system over the 10–60 cm operating range under indoor and outdoor conditions. The evaluation is based on the measured Signal-to-Noise Ratio (SNR), Bit Error Rate (BER), and effective throughput.

The reported values represent the average performance calculated from the individual measurements conducted at transmission distances of 10–60 cm under the illumination conditions tested. Under indoor conditions, the proposed system achieved an average SNR of 38.90 dB, an average BER of 9.41×10^{-5}, and an average effective throughput of 94.60 kbps. Under outdoor conditions, the system achieved an average SNR of 36.54 dB, an average BER of 9.41×10^{-5}, and an average effective throughput of 94.59 kbps. An average BER of 9.41×10^{-5} corresponds to an error ratio equivalent to approximately 9.41 bit errors per 100,000 transmitted bits.

3.1 Indoor Transmission Performance Analysis

The indoor performance of the proposed SDR-based BPSK transceiver was evaluated in terms of Signal-to-Noise Ratio (SNR), Bit Error Rate (BER), effective throughput, and constellation characteristics under ambient illumination levels of 0, 300, and 800 lux over trans-

Table 2: End-to-end multimedia transmission results

Data	Tx Size	Rx Size	Result	
			Tx	*Rx*
Text	Tx_Text Text Document (.txt) Notepad D:\gnurad\sumber 332 KB (340,000 bytes)	Rx_Text Text Document (.txt) Notepad D:\gnurad\BPSK 332 KB (339,968 bytes)	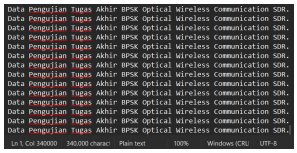	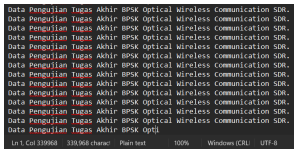
Audio	Tx_Audio MP3 File (.mp3) Media Player D:\gnurad\sumber 4.39 MB (4,610,644 bytes)	Rx_Audio MP3 File (.mp3) Media Player D:\gnurad\BPSK 4.39 MB (4,609,984 bytes)	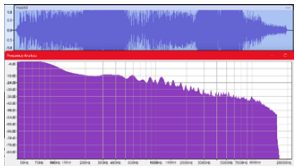	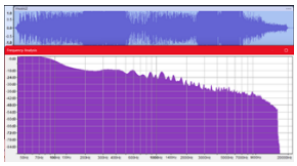
Image	Tx_Image PNG File (.png) Photos D:\gnurad\sumber 827 KB (847,486 bytes)	Rx_Image PNG File (.png) Photos D:\gnurad\BPSK 827 KB (847,424 bytes)		

Table 3: Average performance of the OWC system over the 10–60 cm operating range

Transceiver Model	SNR (dB)	BER	Throughput (kbps)	Environment
BPSK	38.90	9.41×10^{-5}	94.60	Indoor
BPSK	36.54	9.41×10^{-5}	94.59	Outdoor

mission distances ranging from 10 to 70 cm. The corresponding results are presented in Figure 8.

Based on Figure 8a, the received SNR gradually decreases as the transmission distance increases due to free-space optical attenuation, which reduces the optical power received by the BPW34 photodiode. Under the 0-lux condition, the SNR decreases from approximately 46.2 dB at 10 cm to 32.2 dB at 70 cm. Meanwhile, under 300-lux and 800-lux conditions, additional ambient illumination introduces optical noise that further suppresses the SNR, reaching approximately 30.3 dB and 30.1 dB at 70 cm, respectively. These results indicate that the propagation distance is the dominant factor affecting the quality of the received signal, while ambient illumination introduces additional optical noise that further degrades the received SNR.

The BER characteristics for each transmission distance and illumination condition are presented in Figure 8b, while the net throughput is presented in Figure 8c. Across the 10–60 cm transmission range, individual BER measurements remain approximately 9.41×10^{-5} under the indoor illumination conditions tested, while the net throughput remains approximately 94.60 kbps. These results indicate that the proposed system maintains reliable dig-

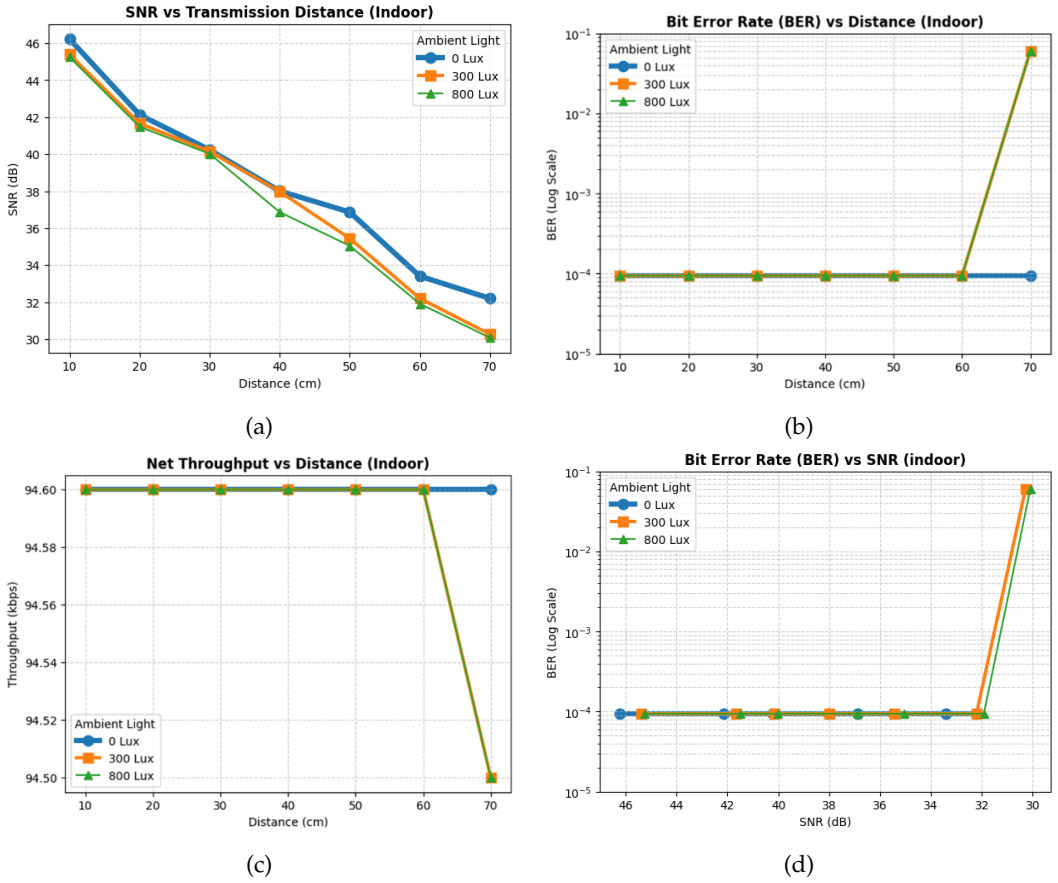

Figure 8: Indoor communication performance of the proposed SDR-based BPSK transceiver: (a) SNR versus transmission distance, (b) BER versus transmission distance, (c) throughput versus transmission distance, and (d) BER versus SNR.

ital communication throughout the 10 to 60 cm operating range under the indoor illumination conditions tested.

At a transmission distance of 70 cm, however, the reduced received optical power, together with increased ambient optical noise, causes the BER to increase under the 300-lux and 800-lux conditions. As a consequence, some received packets fail the CRC32 validation process and are discarded, resulting in a slight reduction in effective throughput. Although communication remains possible at this distance, increased BER reduces the integrity of the data. The received text file can still be reconstructed, although its content is no longer identical to the transmitted file due to accumulated bit errors, whereas the audio and image files cannot be successfully reconstructed.

The relationship between SNR and BER is further illustrated in Figure 8(d). The results show that the BER remains low within the higher-SNR operating region, corresponding to transmission distances of up to 60 cm. When the SNR received decreases to approximately 30 dB at longer transmission distances, the BER increases rapidly, indicating that a lower

SNR significantly reduces the reliability of symbol detection during the BPSK demodulation process.

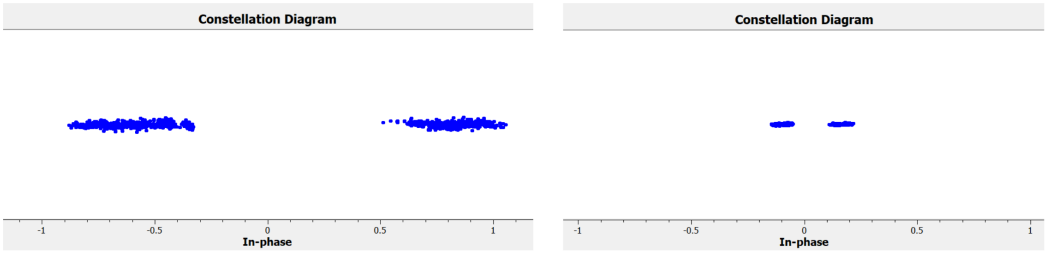

(a) (b)

Figure 9: Received BPSK constellation diagrams under indoor conditions at transmission distances of (a) 10 cm and (b) 70 cm.

The performance of digital phase recovery is further illustrated by the constellation diagrams of I/Q shown in Figure 9. At a transmission distance of 10 cm, the received BPSK symbols form two well-separated constellation clusters, indicating successful symbol synchronization and carrier phase recovery. Even at a maximum transmission distance of 70 cm, the constellation still exhibits two distinguishable symbol clusters, although increased symbol dispersion is observed as a result of reduced received optical power and higher optical noise. These observations indicate that the implemented Symbol Synchronizer and Costas Loop support symbol synchronization and carrier phase recovery over the tested transmission range. However, increased symbol dispersion leads to a higher probability of symbol decision errors, which is consistent with the observed degradation of BER at longer transmission distances.

3.2 Outdoor Transmission Performance Analysis

The outdoor performance of the proposed SDR-based BPSK transceiver was evaluated in terms of Signal-to-Noise Ratio (SNR), Bit Error Rate (BER), effective throughput, and constellation characteristics under ambient solar illumination levels of 10,000, 25,000, and 50,000 lux over transmission distances ranging from 10 cm to 70 cm. The corresponding performance characteristics are presented in Figure 10.

Based on Figure 10a, the received SNR gradually decreases with increasing transmission distance due to free-space optical attenuation and the additional optical noise introduced by solar illumination. At a transmission distance of 10 cm, the highest SNR values are recorded at 44.41 dB, 44.29 dB, and 43.06 dB under ambient illumination levels of 10,000 lux, 25,000 lux, and 50,000 lux, respectively. As the transmission distance increases, the optical power received decreases, resulting in lower SNR values. At the maximum transmission distance of 70 cm, the SNR decreases to 30.60 dB, 30.04 dB, and 30.01 dB, respectively. These results indicate that transmission distance is the dominant factor affecting the received signal quality, while direct solar illumination introduces additional optical noise that further degrades the received SNR.

The BER characteristics for each transmission distance and solar illumination level are presented in Figure 10b, while the net throughput is presented in Figure 10c. Across the

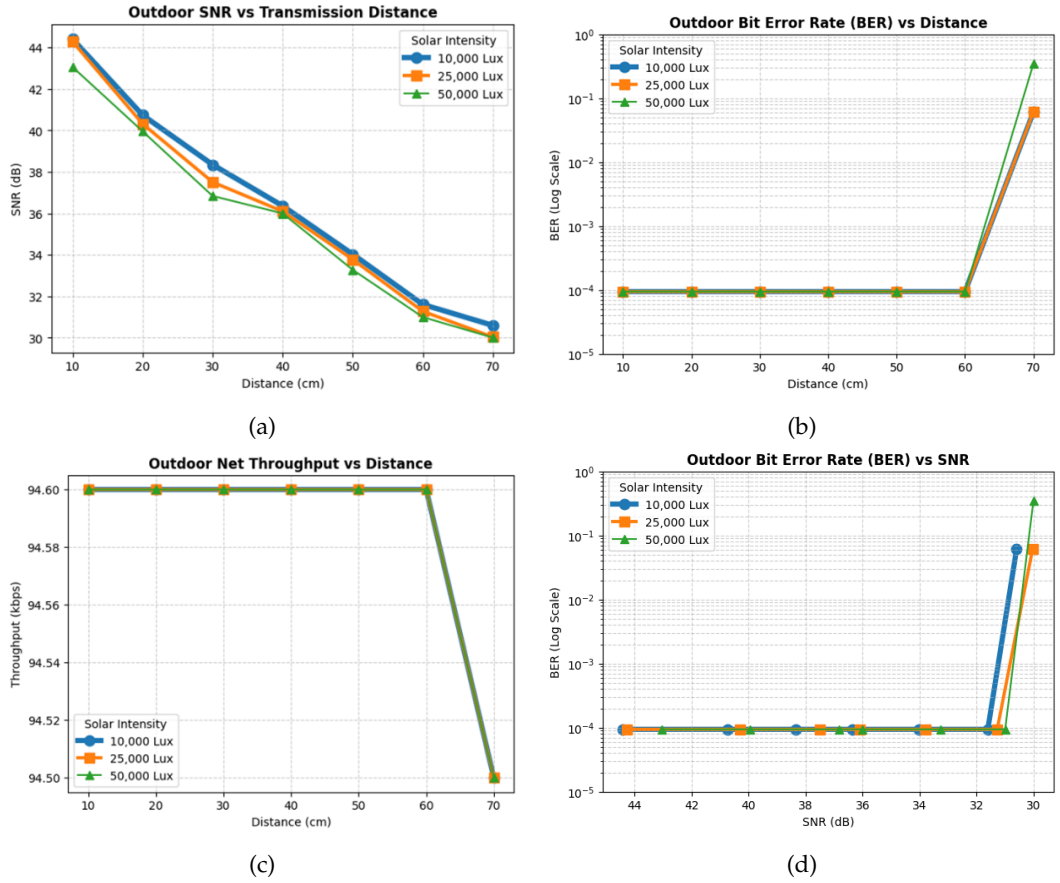

Figure 10: Outdoor communication performance of the proposed SDR-based BPSK transceiver: (a) SNR versus transmission distance, (b) BER versus transmission distance, (c) throughput versus transmission distance, and (d) BER versus SNR.

10–60 cm transmission range, the individual BER measurements remain approximately 9.41×10^{-5} under the tested outdoor illumination conditions, while the net throughput remains approximately 94.59 kbps. These results indicate that the proposed system maintains reliable digital communication within the 10–60 cm operating range despite variations in transmission distance and direct solar illumination.

At the maximum transmission distance of 70 cm, however, reduced received optical power, together with increased ambient optical noise, causes the BER to increase significantly. The BER increases to approximately 6.07×10^{-2} under 10,000 lux and 25,000 lux illumination, and further increases to approximately 3.45×10^{-1} under 50,000 lux illumination. Consequently, a larger number of received packets fail the CRC32 validation process and are discarded, resulting in a slight reduction in effective throughput. Although communication remains possible under these conditions, increased BER reduces the integrity of the data. The received text file can still be reconstructed, although its content is no longer

identical to the transmitted file due to accumulated bit errors, whereas the audio and image files cannot be successfully reconstructed.

The relationship between SNR and BER is further illustrated in Figure 10d. The results show that the BER remains low within the higher-SNR operating region corresponding to transmission distances of up to 60 cm. As the received SNR decreases to around 30 dB at 70 cm, the BER increases rapidly, indicating that lower SNR significantly reduces the reliability of symbol detection during the BPSK demodulation process.

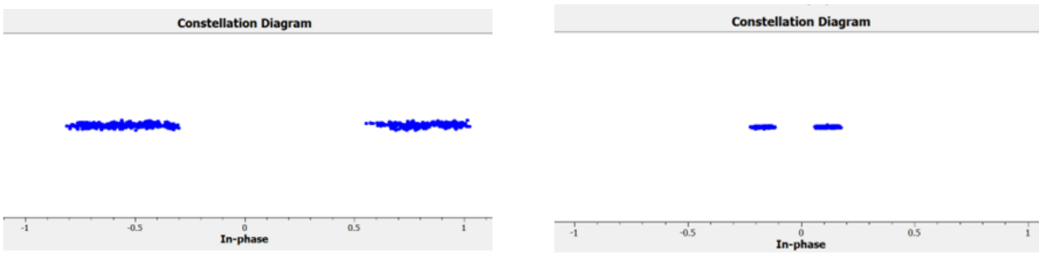

(a) (b)

Figure 11: Received BPSK constellation diagrams under outdoor conditions at transmission distances of (a) 10 cm and (b) 70 cm.

The digital phase recovery performance under outdoor conditions is further illustrated through the I/Q constellation diagrams presented in Figure 11. At a transmission distance of 10 cm, the received BPSK symbols form two well-separated constellation clusters, indicating successful symbol synchronization and carrier phase recovery. At the maximum transmission distance of 70 cm, the constellation still exhibits two distinguishable symbol clusters, although increased symbol dispersion is observed due to reduced received optical power and increased ambient optical noise. These observations indicate that the implemented Symbol Synchronizer and Costas Loop support symbol synchronization and carrier phase recovery over the tested outdoor transmission range. However, the increased symbol dispersion results in a higher probability of symbol decision errors, which is consistent with the observed BER degradation at longer transmission distances.

4 Discussion

4.1 Results Interpretation

The experimental results demonstrate that transmission distance is the dominant factor governing the degradation of the received Signal-to-Noise Ratio (SNR), while ambient optical noise further contributes to performance degradation in both indoor and outdoor environments. Within the practical operating range of 10–60 cm, the received optical power remains sufficient for reliable symbol synchronization and carrier recovery, resulting in a BER of approximately 9.41×10^{-5} and a stable net throughput of approximately 94.60 kbps. Under these conditions, text, audio, and image files are successfully reconstructed without observable corruption, indicating reliable end-to-end communication performance.

The difference between the gross physical-layer bit rate of $500\,\mathrm{kbps}$ and the measured net throughput of 94.60 kbps reflects the overhead and processing associated with the end-

to-end packet-based transmission. The $500\,\mathrm{kbps}$ value represents the gross bit rate determined by the 500 ksymbol/s BPSK symbol rate, whereas the measured throughput represents the successfully delivered multimedia payload. In the implemented flowgraph, each transmission frame has a total length of 338 bytes after the Tagged Stream Mux, consisting of a 64-byte payload, a 250-byte preamble, an 8-byte postamble, and the protocol header information. These additional frame components support synchronization, packet identification, and reliable signal recovery, but reduce the fraction of the physical-layer transmission rate available for payload delivery. In addition, the end-to-end transmission involves packetization, synchronization, packet validation, and multimedia data reconstruction within the GNU Radio processing chain. The measured throughput corresponds to an effective transmission efficiency of approximately 18.92% relative to the 500 kbps gross bit rate. Therefore, the reported 94.60 kbps should be interpreted as the effective end-to-end multimedia throughput rather than the physical-layer transmission rate.

At the maximum transmission distance of 70 cm, reduced received optical power together with increased ambient optical noise causes the received SNR to decrease to approximately 30 dB. Under these conditions, the BER increases significantly, resulting in a higher number of corrupted packets that fail the CRC32 validation process. Consequently, although the received text file can still be reconstructed, accumulated bit errors alter its original content, whereas the audio and image files experience corruption that prevents successful reconstruction. The degradation observed at this distance indicates that the communication link no longer maintains the same level of data integrity achieved within the 10–60 cm operating range.

The I/Q constellation diagrams further support these observations. Even at the maximum transmission distance, the received BPSK symbols remain separated into two distinguishable constellation clusters, indicating that symbol synchronization and carrier phase recovery are still achieved. However, increased symbol dispersion caused by lower received optical power and increased ambient optical noise increases the likelihood of symbol decision errors, which is consistent with the observed BER degradation.

Overall, the measured results indicate that the transmission distance has a stronger effect on communication quality than the tested variations in ambient illumination. For example, the SNR decreases by approximately 14.0 dB between 10 and 70 cm under the 0-lux indoor condition, while the difference between 0 and 800 lux at 70 cm is approximately 2.1 dB. Under outdoor conditions, the SNR decreases by 13.05–14.81 dB between 10 and 70 cm across the tested solar illumination levels, whereas the range of SNR values among the three illumination levels at 70 cm is only approximately 0.59 dB. The nearly constant BER and throughput over 10–60 cm, followed by a sharp BER increase and throughput reduction at 70 cm, further indicate that the reduction in received optical power associated with transmission distance is the primary factor governing the observed performance degradation. Accordingly, the 10–60 cm range represents the practical operating range in which the system maintains stable communication performance and successful multimedia data reconstruction under the tested indoor and outdoor conditions.

4.2 Performance Comparison

Table 4 compares the proposed system with several representative Optical Wireless Communication (OWC) studies employing different modulation schemes, SDR platforms, and optical front-end architectures. Fakidis et al. [14] demonstrated a high-capacity adaptive

Table 4: Performance comparison with previous studies

Work	Transceiver Model	Platform	Optical Link	Max Tested Distance	Max SNR	BER	Throughput	Type of Data Transmitted
[14]	OFDM	Lab Equipment Setup	GaAs VCSEL + Photovoltaic Link	2.0 m	3–6 dB (threshold)	2.2×10^{-3}	784–1041 Mbps	Simultaneous data & power link
[18]	BPSK	USRP SDR	LED + Photodiode	1.6 m	not specified	9.77×10^{-5}	2.5 Mbps	Bitstream test
[16]	QAM-4	HackRF One SDR	Red laser diode + BPW34	3 m	17.83 dB	1.5×10^{-3}	100 kbps	QAM-4 modulated test signal
This work	BPSK	HackRF One SDR	OPV310 VCSEL + BPW34	0.7 m	38.90 dB	9.41×10^{-5}	94.60 kbps	Text, audio, and image

OFDM system using a GaAs VCSEL–photovoltaic link, achieving throughput in the range of 784–1041 Mbps over a transmission distance of 2 m. Banda Sayoc and Gordillo [18] implemented a USRP-based VLC transceiver employing BPSK modulation, reporting a BER of 9.77×10^{-5} at a transmission distance of 1.6 m. Meanwhile, Mozef et al. [16] presented a HackRF One-based VLC transceiver employing QAM-4 modulation with a red laser diode and a BPW34 photodiode, achieving a throughput of 100 kbps over a transmission distance of 3 m. These studies focused primarily on evaluating communication performance under different optical hardware configurations and modulation schemes.

In comparison, the proposed system achieves a BER of 9.41×10^{-5} and an effective throughput of 94.60 kbps over the 10–60 cm reliable operating range. Although its throughput and transmission distance are lower than those reported in several previous studies, the proposed system is designed with a different practical objective: SDR-based infrared LiFi uplink communication with end-to-end multimedia transmission. The system integrates an 850 nm VCSEL, BPW34 photodiode, GNU Radio, and HackRF One SDR, and experimentally evaluates communication performance under indoor and outdoor illumination conditions.

The proposed system, therefore, emphasizes the combination of SDR-based implementation, infrared optical transmission, and end-to-end multimedia reconstruction, rather than maximizing transmission distance or data rate. In addition to BER and throughput, the proposed system is experimentally characterized in terms of SNR, constellation behavior, and multimedia data integrity under different ambient illumination levels. The system successfully supports text, audio, and image transmission within the 10–60 cm reliable operating range, while the experiments also identify the performance degradation occurring at 70 cm. These results demonstrate that the proposed architecture provides a practical SDR-based platform for short-range infrared LiFi uplink communication, particularly for applications where flexible implementation, multimedia transmission, and operation under varying illumination conditions are prioritized over maximum transmission capacity.

4.3 Advantages and Limitations

The proposed SDR-based BPSK transceiver demonstrates several practical advantages for short-range infrared LiFi uplink communication. The use of GNU Radio and SDR hardware provides a software-based signal processing platform in which modulation, synchro-

nization, filtering, and packet-processing functions can be modified without redesigning the optical front-end hardware. This flexibility makes the proposed system suitable for optical wireless communication research and rapid prototyping. Furthermore, the implementation of the Symbol Synchronizer and Costas Loop enables reliable symbol synchronization and carrier phase recovery, allowing the system to maintain reliable communication within the recommended operating range of 10–60 cm under both indoor and outdoor conditions. In addition, the CRC32-based packet validation mechanism improves communication reliability by detecting corrupted packets before payload recovery, thereby helping preserve multimedia data integrity during transmission.

From a practical perspective, the proposed architecture demonstrates the feasibility of using a low-cost SDR-based platform for end-to-end infrared multimedia communication. The successful transmission of text, audio, and image data under different indoor and outdoor illumination conditions indicates that the system can serve as a flexible experimental platform for evaluating infrared optical communication techniques without requiring a fully dedicated communication hardware platform.

Despite these advantages, the proposed system also exhibits several limitations. The reliable operating distance is limited to approximately 60 cm because the received optical power decreases as the transmission distance increases, leading to SNR degradation and higher BER. Although communication remains possible at a transmission distance of 70 cm, the increased BER reduces multimedia data integrity. The received text file can still be reconstructed, although its content is no longer identical to the transmitted data due to accumulated bit errors, whereas the audio and image files become corrupted and cannot be successfully reconstructed. Furthermore, the receiver front-end does not incorporate an Automatic Gain Control (AGC) mechanism, making the receiver more sensitive to variations in ambient illumination, particularly under strong outdoor solar illumination. The current implementation also employs a fixed BPSK-based transmission configuration and does not yet incorporate adaptive modulation or error-correction mechanisms.

Future research may therefore focus on improving receiver sensitivity and communication robustness through the integration of optical collimation lenses, narrow-band optical filters, Automatic Gain Control (AGC), adaptive synchronization algorithms, and Forward Error Correction (FEC) techniques. Higher-order modulation schemes may also be investigated to improve spectral efficiency and increase the achievable data rate. These enhancements are expected to extend the practical communication distance, improve the robustness against ambient optical interference, and support reliable multimedia transmission under more challenging environmental conditions. Further evaluation using mobile transmitter–receiver scenarios would also be beneficial to assess the applicability of the proposed architecture to real-time LiFi communication.

5 Conclusion

This paper presented the design, implementation, and experimental evaluation of an SDR-based BPSK transceiver for infrared LiFi uplink communication. The proposed system successfully demonstrated end-to-end multimedia transmission and reconstruction of text, audio, and image files using GNU Radio, HackRF One SDR, and an infrared optical wireless link. The experimental results showed that the system maintained reliable communication within the recommended operating distance of up to 60 cm in both indoor and

outdoor environments, achieving a BER of approximately 9.41×10^{-5} and a stable net throughput of approximately 94.60 kbps. The results further demonstrated that transmission distance is the dominant factor affecting communication performance, while ambient illumination introduces additional optical noise that accelerates performance degradation. Beyond the recommended operating distance of 60 cm, reduced received optical power caused SNR degradation and a significant increase in BER, leading to reduced multimedia data integrity. Although the received text file could still be reconstructed, its content was no longer identical to the transmitted data due to accumulated bit errors, whereas the audio and image files became corrupted and could not be successfully reconstructed. Overall, the experimental results confirm the feasibility of implementing a low-cost SDR-based infrared LiFi uplink system for short-range optical wireless communications.

The proposed architecture also provides a practical software-based platform for investigating infrared LiFi communication and multimedia transmission under varying illumination conditions. These findings support the potential use of SDR-based optical wireless platforms for flexible prototyping and experimental evaluation of future LiFi systems. Future research should investigate higher-order modulation techniques to improve data-rate capability, adaptive synchronization, and receiver processing to enhance robustness under varying channel conditions, and optical front-end improvements to extend the practical transmission distance. Further evaluation in real-time mobile transmitter–receiver scenarios is also required to assess the applicability of the proposed architecture to dynamic LiFi communication environments.

Declaration

Conflict of Interest

The authors declare that they have no known competing financial interests or personal relationships that could have appeared to influence the work reported in this paper.

Generative AI Declaration

During the preparation of this work, the author(s) used AI tools (such as ChatGPT) solely for language translation, grammatical correction, and polishing the text clarity. The author(s) reviewed and edited the content as needed and take full responsibility for the content of the publication.

List of Contribution

1. Eril Mozef: Conceptualization, Formal analysis, Funding acquisition, Methodology, Project administration, Resources, Supervision, Validation, Visualization, Writing – Review & Editing.
2. Naufal Daffa Naafilah: Data curation, Formal analysis, Investigation, Methodology, Software, Validation, Visualization, Writing – Original Draft, Writing – Review & Editing.
3. Hepi Ludiyati: Resources, Validation, Visualization, Writing – Review & Editing.
4. Enceng Sulaeman: Validation, Visualization, Writing – Review & Editing.

References

[1] T. C. Yu, W. T. Huang, W. B. Lee, C. W. Chow, S. W. Chang, and H. C. Kuo, "Visible light communication system technology review: Devices, architectures, and applications," *Crystals*, vol. 11, p. 1098, Sept. 2021.

[2] A. Celik, I. Romdhane, G. Kaddoum, and A. M. Eltawil, "A top-down survey on optical wireless communications for the internet of things," *IEEE Communications Surveys & Tutorials*, vol. 25, no. 1, pp. 1–45, 2023.

[3] L. Bravo Alvarez, S. Montejo-Sánchez, L. Rodríguez-López, C. Azurdia-Meza, and G. Saavedra, "A review of hybrid VLC/RF networks: Features, applications, and future directions," *Sensors*, vol. 23, p. 7545, Aug. 2023.

[4] M. Z. Chowdhury, M. K. Hasan, M. Shahjalal, M. T. Hossan, and Y. M. Jang, "Optical wireless hybrid networks: Trends, opportunities, challenges, and research directions," *IEEE Communications Surveys & Tutorials*, vol. 22, no. 2, pp. 930–966, 2020.

[5] X. Zhang, G. Klevering, X. Lei, Y. Hu, L. Xiao, and G.-H. Tu, "The security in optical wireless communication: A survey," *ACM Computing Surveys*, vol. 55, pp. 1–36, July 2023.

[6] S. B. Aboagye, A. R. Ndjiongue, T. M. N. Ngatched, O. A. Dobre, and H. V. Poor, "RIS-assisted visible light communication systems: A tutorial," Apr. 2022.

[7] C. Chen, D. A. Basnayaka, A. A. Purwita, X. Wu, and H. Haas, "Wireless infrared-based LiFi uplink transmission with link blockage and random device orientation," *IEEE Transactions on Communications*, vol. 69, pp. 1175–1188, Feb. 2021.

[8] D. F. Fonseca, M. S. Mir, B. G. Guzman, and D. Giustiniano, "Visible light or infrared? modulating LiFi for dual operation in the visible and infrared spectra," in *2023 18th Wireless On-Demand Network Systems and Services Conference (WONS)*, (Madonna di Campiglio, Italy), pp. 47–50, Jan. 2023.

[9] M. Dehghani Soltani, E. Sarbazi, N. Bamiedakis, P. De Souza, H. Kazemi, J. M. H. Elmirghani, I. White, R. V. Penty, H. Haas, and M. Safari, "Safety analysis for laser-based optical wireless communications: A tutorial," *Proceedings of the IEEE*, vol. 110, pp. 1045–1072, Aug. 2022.

[10] X. Fang, Y. Zhu, X. Cai, W. Hu, Z. He, S. Yu, and F. Zhang, "Overcoming laser phase noise for low-cost coherent optical communication," *Nature Communications*, vol. 15, p. 6339, July 2024.

[11] S. Liu, X. You, J. Chen, *et al.*, "Real-time implementation of hybrid visible light/infrared communications supporting full-range dynamic dimming control," *IEEE Photonics Journal*, vol. 16, pp. 1–14, Feb. 2024.

[12] I. N. O. Osahon, I. Kostakis, D. Powell, W. Meredith, M. Missous, H. Haas, J. Tang, and S. Rajbhandari, "Neural network equalisation for high-speed eye-safe optical wireless communication with 850 nm SM-VCSELs," *Photonics*, vol. 11, p. 772, Aug. 2024.

[13] O. Faruq, K. R. S. Rahman, N. Jahan, S. Rokoni, and M. Rabeya, "Li-Fi technology based long range free-space optics data transmit system evaluation," *EAI Endorsed Transactions on Mobile Communications and Applications*, vol. 7, p. e3, May 2023.

[14] J. Fakidis, H. Helmers, and H. Haas, "Simultaneous wireless data and power transfer for a 1-gb/s GaAs VCSEL and photovoltaic link," *IEEE Photonics Technology Letters*, vol. 32, pp. 1277–1280, Oct. 2020.

[15] H.-T. Cheng, Y.-C. Yang, T.-H. Liu, and C.-H. Wu, "Recent advances in 850 nm VCSELs for high-speed interconnects," *Photonics*, vol. 9, p. 107, Feb. 2022.

[16] E. Mozef, D. Wijaya, H. Ludiyati, E. Sulaeman, H. Madiawati, M. Y. Firdaus, *et al.*, "Hardware implementation of RF-to-optical and optical-to-RF converters for a laser-driven VLC system based on HackRF One SDR," *E3S Web of Conferences*, vol. 664, p. 01009, 2025.

[17] GNU Radio, "File transfer using packet and BPSK." Accessed: June 8, 2026.

[18] O. R. Banda Sayco and A. Cartagena Gordillo, "Design and implementation for a USRP-based visible light communications transceiver," in *2019 UNSA International Symposium on Communications (UNSA ISCOMM)*, (Arequipa, Peru), pp. 1–5, 2019.